Quantitative model of cellulite: Three-dimensional skin surface topography, biophysical characterization, and relationship to human perception

LOLA K. SMALLS, CAROLINE Y. LEE,
JENNIFER WHITESTONE, W. JOHN KITZMILLER,
R. RANDALL WICKETT, and MARTY O. VISSCHER, *The Skin
Sciences Institute, Cincinnati Children's Hospital Research Foundation,
Cincinnati, OH (L.K.S., C.Y.L., W.J.K., R.R.W., M.O.V.); Colleges
of Pharmacy (L.K.S., R.R.W.) and Medicine (W.J.K.), University of
Cincinnati, Cincinnati, OH 54267; and Total Contact, Inc.,
Germantown, OH 45327 (J.W.).*

Synopsis

Gynoid lipodystrophy (cellulite) is the irregular, dimpled skin surface of the thighs, abdomen, and buttocks in 85% of post-adolescent women. The distinctive surface morphology is believed to result when subcutaneous adipose tissue protrudes into the lower reticular dermis, thereby creating irregularities at the surface. The biomechanical properties of epidermal and dermal tissue may also influence severity. Cellulite-affected thigh sites were measured in 51 females with varying degrees of cellulite, in 11 non-cellulite controls, and in 10 male controls. A non-contact high-resolution three-dimensional laser surface scanner was used to quantify the skin surface morphology and determine specific roughness values. The scans were evaluated by experts and naïve judges (n = 62). Body composition was evaluated via dual-energy x-ray absorptiometry; dermal thickness and the dermal-subcutaneous junction were evaluated via high-resolution 3D ultrasound and surface photography under compression. Biomechanical properties were also measured. The roughness parameters Svm (mean depth of the lowest valleys) and Sdr (ratio between the roughness surface area and the area of the xy plane) were highly correlated to the expert image grades and, therefore, designated as the quantitative measures of cellulite severity. The strength of the correlations among naïve grades, expert grades, and roughness values confirmed that the data quantitatively evaluate the human perception of cellulite. Cellulite severity was correlated to BMI, thigh circumference, percent thigh fat, architecture of the dermal-subcutaneous border (ultrasound surface area, red-band SD from compressed images), compliance, and stiffness (negative correlation). Cellulite severity was *predicted* by the percent fat and the area of the dermal-subcutaneous border. The biomechanical properties did not significantly contribute to the prediction. Comparison of the parameters for females and males further suggest that percent thigh fat and surface area roughness deviation are the distinguishing features of cellulite.

INTRODUCTION

Gynoid lipodystrophy (cellulite), the unattractive cottage cheese-like dimpling of the thighs, abdomen, and buttocks, affects 85% of post-adolescent women (1,2). Cellulite treatment is a high priority for the pharmaceutical and cosmetic industries (2–10). Products (11–15), supplements (16), and massage techniques (8,9) purport to treat cellulite, presumably by reducing the appearance of the dimpled, lumpy skin. The uneven skin surface texture is attributed to the three-dimensional (3D) architecture of the hypodermal connective tissue (14,17–20). In females, fat cell chambers, "papillae adiposae," are sequestered by connective tissue septa, positioned in a radial and arched manner and anchoring the dermis to the muscle fascia. The subcutaneous fat cell chambers bulge into the dermis, thereby changing the skin surface appearance (13). The literature on the etiology of cellulite and the effectiveness of treatments to ameliorate the condition is limited (4,6,14,16,21), given the prevalence. The surface features of cellulite are believed to result when subcutaneous adipose tissue protrudes into the lower reticular dermis, thereby creating irregularities at the epidermal surface. The biomechanical properties of the epidermis and dermis may also influence the severity. Cellulite is not specific to overweight females, but added weight may cause enlargement of the fat lobules, further protrusion into the dermis, and exacerbation of the condition (2,17). Weight loss is reported to diminish cellulite, but it may not alter the underlying dermal-subcutaneous structures (17,19). Identification of key factors responsible for the visual appearance of cellulite will help to facilitate the development and selection of effective treatments.

We conducted a set of noninvasive biophysical measurements of the cellulite-affected tissue and determined the specific factors that contribute to cellulite severity. The surface morphology was quantified with a non-contact three-dimensional laser scanning system to generate surface roughness parameters and provide a standardized measure of severity. In the literature, cellulite severity is generally evaluated with various visual and photographic methods, although accepted standards have not yet emerged. We related the technical measures of severity to naïve and subject assessment using a 0–9 category scale. Quantitative, reproducible methods will facilitate effective comparison of treatments across studies. Furthermore, treatment effectiveness will be judged by the patient/consumer based on the impact on cellulite severity and appearance. Ultimately, evaluation methods must be linked to human perception of severity and change.

MATERIALS AND METHODS

SUBJECTS

Fifty-one females with visible cellulite were recruited from several weight-loss programs (medication, liquid diet, Weight Watchers®, and bariatric surgery). Eleven females without visible cellulite were controls. Individuals who were pregnant, had an active skin condition (e.g., rash, wound) on the thigh, or had been treated for cellulite within three months were excluded from participation. The Institutional Review Boards of Cincinnati Children's Hospital Medical Center and the University of Cincinnati approved the research protocol. All subjects provided written informed consent for participation.

Ten males, matched to the female subjects for BMI and age, were recruited to determine the effect of gender on the morphological and biophysical characteristics of the thigh. All subjects provided written informed consent. The thigh areas were shaved with electric clippers prior to measurements.

Sixty-two females without prior knowledge of the cellulite research were recruited as naïve judges from the general population. They evaluated the thigh images for severity, using a 0–9 category scale. The study subjects provided written consent for evaluation of their cellulite images.

THREE-DIMENSIONAL SKIN SURFACE TOPOGRAPHY

Three-dimensional (3D) skin surface data were obtained with a Cyberware Rapid 3D Digitizer (Cyberware, Inc., Monterrey, CA) laser scanner mounted on a linear platform and controlled by CyScan data acquisition software (Figure 1). The scanner operates on the principle of triangulation. As a helium-neon laser light source passes through two cylindrical lenses, the resulting vertical plane of light projects onto the surface of the object. The highlighted profile is reflected from the image mirrors to a video sensor and digitized in a raster fashion to determine the two-dimensional (2D) coordinates of 256 points along the profile surface. The scanner moves along a linear trajectory, performing
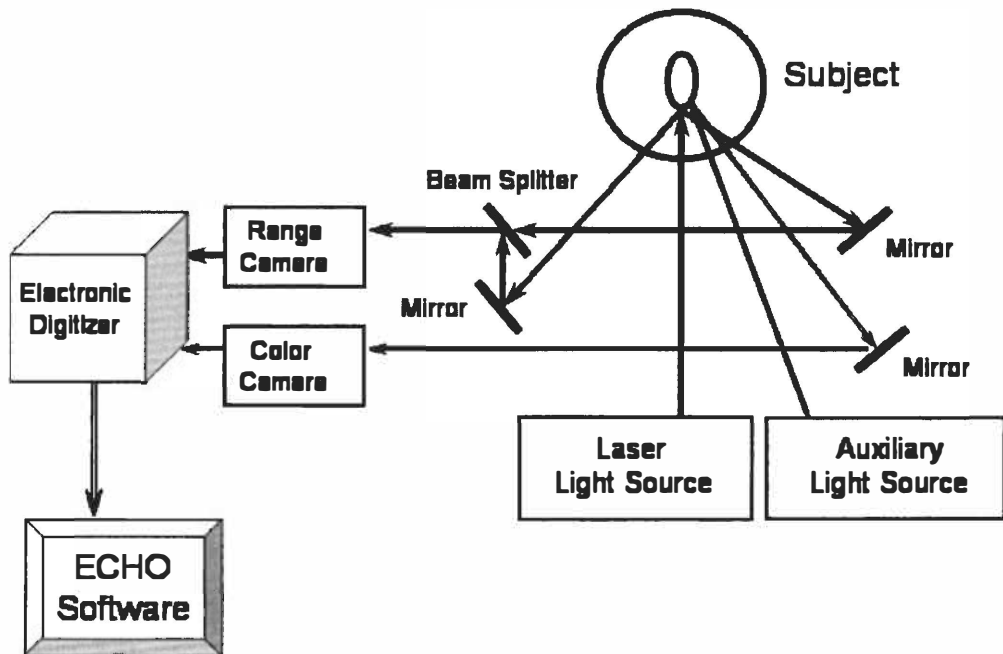

Figure 1. Three-dimensional laser-scanning process. The scanner operates on the principle of triangulation. As a helium-neon laser light source passes through two cylindrical lenses, the resulting vertical plane of light projects onto the surface of the object being scanned. The highlighted profile is reflected from the image mirrors to a video sensor and digitized in a raster fashion to determine the two-dimensional (2D) coordinates of 256 points along the profile surface. The scanner moves along a linear trajectory performing 512 individual surface contour scans in equal increments.

512 individual surface contour scans in equal increments. Trigonometric calculations of the 2D coordinates to three-dimensional (3D) space are performed.

The outer aspects of both thighs were scanned (402 × 170 mm in <40 sec at 0.5 × 0.38 mm planar resolution) while subjects sat on a level surface with knees bent at a 90° angle. The scanner was raised and lowered with the aid of a special motor-controlled platform to allow accurate positioning of the subject within the scan area. The quantitative surface roughness parameters were calculated from the scan data with a customized version of TrueMap Software (TrueGage, N. Huntingdon, PA). The images were first processed to remove non-cellulite features. The form removal utility applied an LS third-order polynomial equation to remove the thigh curvature. The filtering utility, set at 0.25 mm, removed noise due to movement, hair, and varicose veins. Remaining anomalies were deleted with an outlier routine. The surface roughness parameters (Table I) were calculated for the region of interest (10.7 × 11.3 cm, center of the thigh) (22).

VISUAL SCORING OF CELLULITE

Expert image scores. Three research team members reviewed 66 3D laser scans (gray scale images on a black background) that covered the range of severities observed in the general population. They identified the cellulite features and developed a ten-point classification scale of cellulite severity (0–9) wherein 0 represented no cellulite; 1, 2, and 3 indicated varying degrees of slight cellulite; 4, 5, and 6 indicated moderate cellulite; and 7, 8, and 9 indicated severe cellulite. We selected ten images, representing each point (0–9), for evaluation by naïve judges and established the ten images as the expert image grading scale.

Table I
3D Surface Roughness Parameters (22)

Parameter	Description
Sa	Average roughness (mm): Average of the absolute distances of the surface profile from the reference plane
Sq	Root-mean-square roughness (mm): Width or variance of the amplitude distribution function
Sp	Maximum profile peak height (mm): Height of the highest profile peak above the reference plane
Sv	Maximum profile valley depth (mm): Depth of the lowest profile valley below the reference plane
St	Maximum height of profile (mm): The vertical distance from the highest peak to the deepest valley (St = Sp + Sv)
Ssk	Skewness (mm): Symmetry of the roughness profile variation about its mean
Sku	Kurtosis (mm): Spikiness of the roughness profile
Spm	Mean maximum profile peak height (mm): Mean height of the highest peaks over the entire surface
Svm	Mean maximum profile valley depth (mm): Mean depth of the lowest valleys over the entire surface
Sz	Mean maximum height of profile (mm): Mean vertical distance from the highest peaks to the lowest valleys over the entire surface (Sz = Spm + Svm)
Sdr	Surface area ratio (%): The ratio between the roughness surface area and the area of the flat xy plane. For a flat surface, the surface area and the xy plane area are equal, and Sdr = 0%

Live visual grades. The lateral thighs were evaluated with the subject positioned on a bicycle seat (to avoid thigh compression) with the knees bent at 90° angles. A trained judge scored the outer aspect of each thigh using the following scale: 0 (smooth, no dimples), 1 (shallow, small visible dimples, few and sparsely located), 2 (moderate number of visible dimples, some large), 3 (large number of dimples, many large, over most of the surface, cottage cheese appearance), and 4 (wide, deep visible dimples over entire thigh, very prominent cottage cheese appearance). Half-point increments were used for intermediate conditions, resulting in ten increments: 0, 0.5, 1.0, 1.5, 2.0, 2.5, 3.0, 3.5, 4.0, and 4.5 (for grades higher than 4.0).

MEASUREMENTS

Weight, height, and thigh circumference were measured using a standard hospital scale with height bar and measuring tape. Sites at the center lateral thighs were demarcated with a 2-cm diameter area centered within a 5-cm diameter circle.

DUAL-ENERGY X-RAY ABSORPTIOMETRY (DEXA)

Total and regional body composition (lean and fat mass) was measured with a dual-energy x-ray absorptiometry (DEXA) total body scanner (Hologic Inc., San Francisco, CA) at the body core composition laboratory of the General Clinical Research Center of Cincinnati Children's Hospital Medical Center. Fat percentages were calculated for the total body, thigh, thigh subregion (area of ultrasound and biomechanical measurements), android (torso), and gynoid (hip/thigh), using joints as landmarks. The body fat distribution was calculated from the android/gynoid fat mass ratio, an index of the fat allocation amid the torso and hip/thigh regions (23).

ULTRASOUND

Dermal thickness (mm) and the dermal-subcutaneous junction surface area (mm^2) of the thigh sites were determined using the Dermascan C® Version 3 (Cortex Technology, Hadsund, Denmark) with a 20 MHz 3D probe (24). A 22.4 × 22.4 mm area was scanned with an interslice distance of 0.2 mm, providing 112 B-scans (2D images). The acoustic velocity of the instrument was set to 1580 m/s (24). The mean dermal thickness (112 B-Scans) was determined with the Dermascan C® software to define the outer boundary of the epidermis and the inner dermal/subcutaneous fat boundary. The surface area of the 3D dermal/subcutaneous junction was reconstructed by manually delineating the dermal/subcutaneous border from 50 consecutive B-Scans ($224 \ mm^2$ area or 50 scans × 0.2 mm *z-dir* × 22.4 mm *y-dir*).

SURFACE TEXTURE WITH PHOTOGRAPHY

Surface texture under compression was measured with an Accentuated Cellulite Imaging System (ACIS, Procter and Gamble, Cincinnati, OH). The thigh was compressed with gripping handles to 11.6 mm from a starting point of zero. Moisturizing lotion (Oil of Olay Beauty Fluid, Procter and Gamble, Cincinnati, OH) was applied prior to the measurement to eliminate confounding the effects of dry skin. Digital images were

captured, color corrected, and processed (Optimas software). A center region (570 × 210 mm) was analyzed to eliminate edge effects. Changes in the color intensity of adjacent pixels provided an output parameter related to shadowing in cellulite dimples under compression and designated as the red-band standard deviation (red-band SD).

BIOMECHANICAL PROPERTIES

The biomechanical properties were measured at the thigh site (2-cm diameter area) using the BTC-2000™ (SRLI Technologies, Nashville, TN) through two cycles over 2 cm at a pressure of 10 mmHg/sec for 15 seconds (150 mmHg, 200 mbar) with five seconds of relaxation between cycles. The measured properties were laxity (acute elastic deformation), laxity % (percent, indicates slack or looseness), elastic deformation (total displacement at maximum pressure), stiffness (slope of the stress/strain curve; higher value indicates tighter skin), energy absorption (area under the stress/strain curve, entire deformation response; higher values indicate more compliant skin), elasticity (reverse deformation by full-pressure release), and elasticity % (elasticity/elastic deformation × 100%; higher values indicate more elastic skin) (25).

NAIVE JUDGE CELLULITE IMAGE ASSESSMENT

High-contrast (gray scale) images were viewed on black backgrounds to allow the judge to focus on the image and distinguish the skin surface features. The length of time for the evaluation was optimized to minimize fatigue and maximize response fidelity. At the start of a session, the judge was given descriptors of cellulite (lumps, bumps, dimples, ripples, cottage cheese appearance) and instructed to ignore non-cellulite features (e.g., vertical bands, specks). Responses were made using a 0–9 category scale (Table II).

Four assessment schemes (A–D) were used to randomize presentation and ensure that the question sequence was removed as a variable in scoring cellulite severity. Judges first viewed single images to obtain a frame of reference and then evaluated the ten single images of the expert image grading scale. The use of pair-wise comparisons is more effective than subjective rating scales in medical imaging since it allows observers to detect small differences in image quality (26). We used a modified version of the two-alternative forced-choice (TAFC) method in which judges scored each image within a pair. The method assumes that the image with the higher score has the more severe condition (26). Twenty-five randomized pairs of varying differences in severity were evaluated to determine the threshold of incremental discrimination (i.e., grade 1 vs grade 7, a six-increment difference). Pairs of identical images were included as controls.

STATISTICAL ANALYSIS

The data were analyzed using the Sigma Stat Software (SPSS, Inc.), with a significance level of $p \leq 0.05$. Results were represented as mean ± SD and mean ± SEM. Student's

Table II
Ten-Point Category Scale

None	Slight cellulite			Moderate cellulite			Severe cellulite		
●	1	2	3	4	5	6	7	8	9

t-test was used for comparison of two different groups. Correlation coefficients were computed using Pearson Product Moment or Spearman procedures (non-normally distributed data) in order to evaluate relationships among parameters. Multiple linear regression analyses were carried out to determine the ability of a combination of independent variables to predict the dependent variable.

RESULTS

QUANTITATION OF CELLULITE SEVERITY

Selection criteria for the ten final images of the 0–9 expert image grading scale (Figure 2) included depth of dimples, area of coverage, and cottage-cheese-like appearance. Correlation of the expert image grades with the surface roughness parameters (Table III) indicated the highest association (correlation coefficient = 0.86, p = 0.008) for Svm (Figure 3). Parameter Sdr was also highly correlated with the expert image score (correlation coefficient = 0.86, p = 0.002). Inclusion of the non-correlated variables Ssk and Sku in the multiple linear regression analysis did not add significantly to either model.
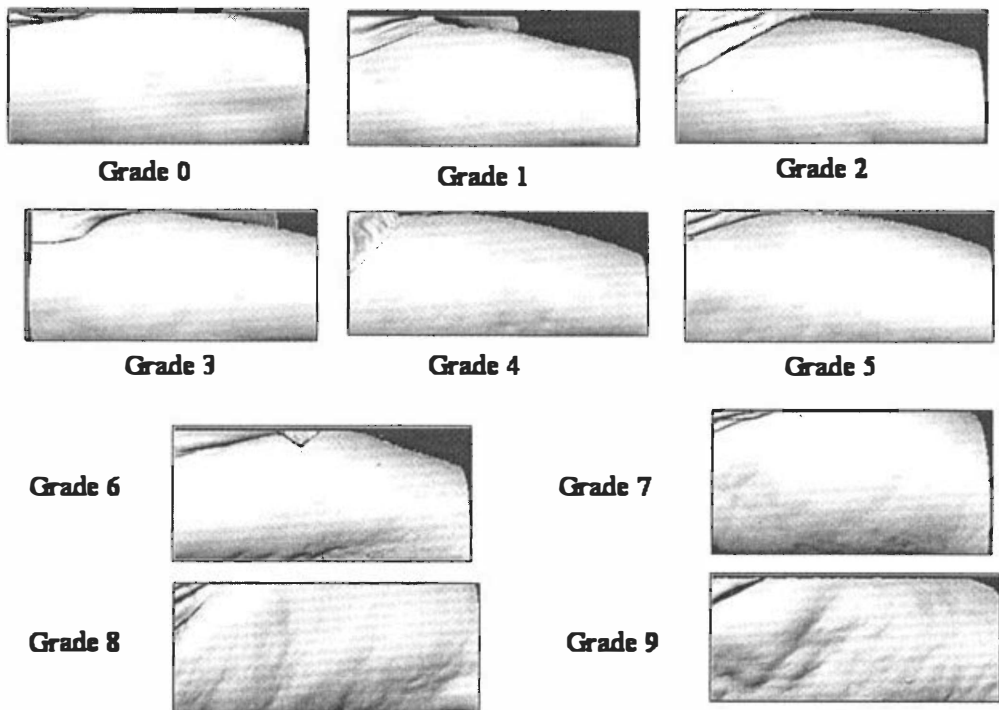

Figure 2. Expert image grading scale. Three experts reviewed 66 3D laser scans that covered the range of severities observed in the general population, identified the cellulite features, and developed a ten-point classification scale of cellulite severity (0–9). A grade of 0 represented no cellulite; 1, 2, and 3 indicated varying degrees of slight cellulite; 4, 5, and 6 were moderate; and 7, 8, and 9 were severe. Ten images, representing each point (0–9), were established as the expert image grading scale and used for evaluation by naïve judges.
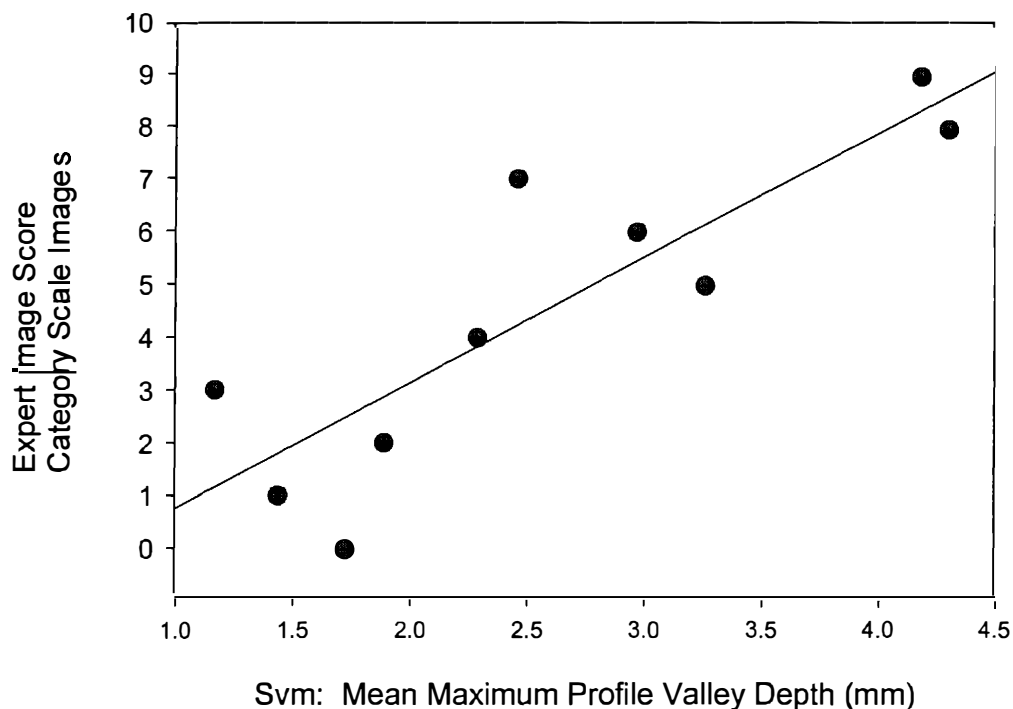
Figure 3. Skin surface roughness versus expert image score. Skin surface roughness parameters were quantified with TrueMap software for each of the ten images on the expert image grading scale. Parameter *Svm* had the highest correlation (r = 0.86, p = 0.001) to the expert image grade (n = 10) and was, therefore, considered to be a quantitative measure of cellulite severity.

Similarly, weight, age, and the interaction term (weight · age) did not affect either *Svm* or *Sdr*. For *Svm,* the equation was: *Image Score = –1.66 + (2.4 · Svm),* with values of R, R^2, and adjusted R^2 of 0.86, 0.75, and 0.71, respectively. For *Sdr,* the equation was *Image Score = 1.25 + (388 · Sdr),* with values of R, R^2, and adjusted R^2 of 0.86, 0.73, and 0.70, respectively. The live expert visual grades (using the ten-point 0–4.5 scale) for the ten thighs in the expert image scale were highly correlated to the expert image scores (r = 0.92, Table III). The highest correlation was for *Sdr* (r = 0.89), suggesting that this parameter is sensitive to human visual perception.

While both the naïve and expert judges used the 0–9 scale, the naïve judges rated the images lower than the experts did, presumably because they were processing the data in a bottom-up fashion, i.e., perceptions were formed based on the data in the images. The naïve judge mean scores and the expert grades for the ten images were highly correlated (r = 0.96) and not significantly different. *Svm* and *Sdr* had the highest correlations to expert and naïve scores (r ≥ 0.86) (Figure 4). The two groups agreed on the paired assessments, although the experts noted larger differences. This result is not surprising, since the experts established the image grading scale. The experts used top-down processing, i.e., perceptions were formed based upon expectations and from previous knowledge with the range of severity.

Table III
Cellulite Score and Surface Roughness Parameter Correlations (n = 10)

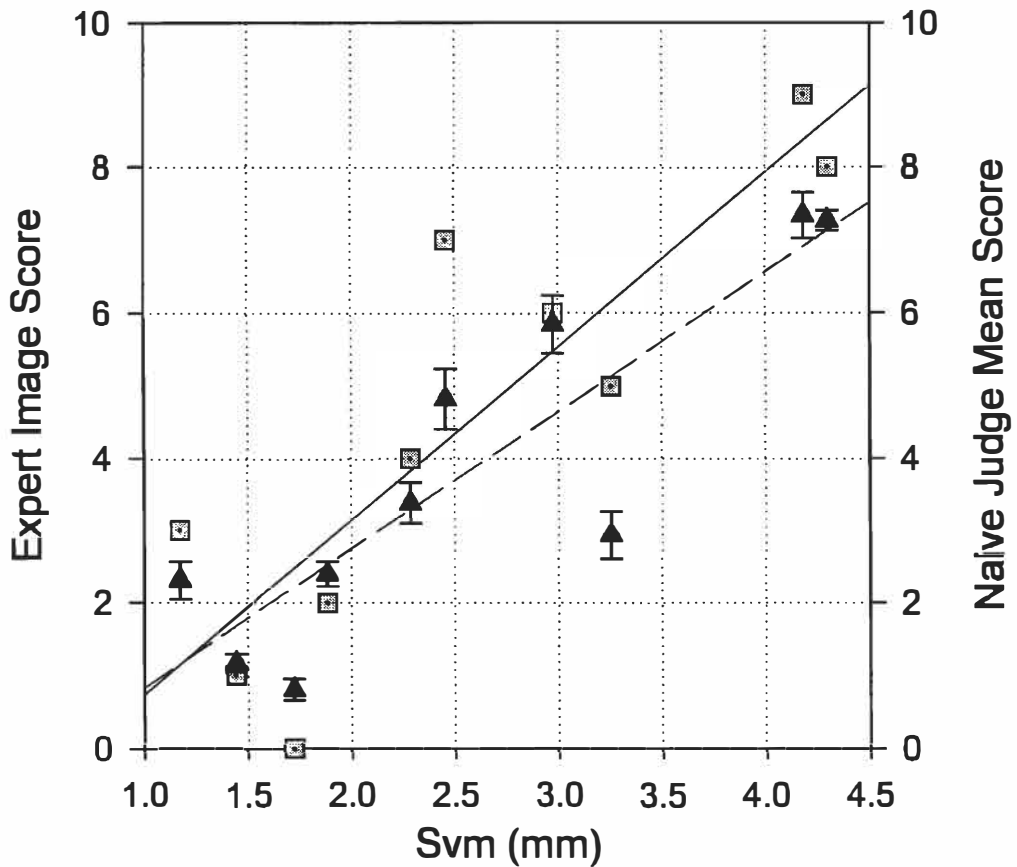|	Visual score	Sa	Sq	Sp	Sv	St	Ssk	Sku	Spm	Svm	Sz	Sdr
Expert image score	0.92	0.76	0.75	0.67	0.67	0.76	0.39	−0.32	0.78	0.86	0.83	0.86
(r, *p* value)	0.00	0.011	0.013	0.033	0.033	0.011	0.269	0.361	0.008	0.001	0.003	0.002
Live visual score		0.82	0.77	0.79	0.51	0.71	0.56	−0.71	0.86	0.83	0.86	0.89
(r, *p* value)		0.002	0.007	0.004	0.126	0.019	0.081	0.019	0.000	0.000	0.000	0.000

Figure 4. Quantitative roughness evaluation and human image assessment. The expert grades and naïve-judge mean scores for the ten expert-image grading scale images are plotted versus the quantitative cellulite-severity parameter *Svm*. The expert and naïve scores were highly correlated ($r = 0.96$) and not significantly different. Both *Svm* and *Sdr* had the highest correlations to expert and naïve scores ($r \geq 0.86$).

BIOPHYSICAL CHARACTERIZATION OF CELLULITE

Fifty-six females completed the study measurements. The mean BMI (kg/m^2) was 34.6 $\pm$ 8 (range 21–57), and the mean weight was 204 $\pm$ 52 (range 128–331). The mean age was 44.3 ± 8 (range 21–60). For the ten males, the mean BMI was 33.2 ± 6 kg/m^2 and the mean age was 41.8 ± 11.2 years.

Table IV shows the results (mean $\pm$ standard error, range) for all of the biophysical evaluations (females and males). Correlations were found between expert image grades and quantitative roughness. *Svm, Sz,* and *Spm* had the highest correlations with image score (females), with coefficients of 0.69 ($p < 0.001$), 0.68 ($p < 0.001$), and 0.62 ($p < 0.001$), respectively.

The biophysical features that related to cellulite severity were identified from the relationships among all measurements (Table V, coefficients of ≥ 0.4 or higher, $p < 0.05$). Cellulite severity, as measured by surface roughness (*Svm*) or live visual grade, was correlated to BMI (weight), thigh circumference, percent thigh fat, and the architecture

Table IV
Morphological, Biophysical, and Anthropomorphic Measurements of Cellulite

	Females	N = 54	Males	N = 10
	Mean ± SE	Range	Mean ± SE	Range
Anthropomorphic data				
Weight (lb)	205.4 ± 7.0	128–331	225.6 ± 12.3	168–290
BMI	34.9 ± 1.2	21.3–56.8	33.2 ± 1.9	26.8–43.3
Age (years)	44.4 ± 1.2	21–60	41.8 ± 3.5	25–57
Thigh circumference (in)	26.9 ± 0.5	21–35	26.0 ± 0.8	23.0–30.5
Cellulite morphology				
Visual grade	1.0 ± 0.2	0.0–4.0	0.2 ± 0.1	0.0–1.0
Expert image score	4.7 ± 0.4	0.0–9.0	3.8 ± 0.8	0.0–7.0
Sa	1.1 ± 0.1	0.3–2.1	0.8 ± 0.1	0.4–1.3
Sq	1.4 ± 0.1	0.4–2.6	1.0 ± 0.1	0.5–1.6
Sp	3.9 ± 0.2	1.2–8.7	3.4 ± 0.4	1.8–5.9
Sv	5.2 ± 0.3	1.5–12.9	4.4 ± 0.5	2.7–8.0
St	9.1 ± 0.4	3.1–17.9	7.8 ± 0.8	5.0–12.8
Ssk	−0.2 ± 0.1	−1.5–0.8	−0.2 ± 0.1	−1.2–0.1
Sku	3.8 ± 0.2	2.2–7.1	4.2 ± 0.7	2.3–8.9
Spm	2.6 ± 0.1	1.0–4.8	2.1 ± 0.2	1.2–3.4
Svm	2.8 ± 0.2	1.0–7.1	2.3 ± 0.2	1.7–3.6
Sz	5.4 ± 0.3	2.0–11.8	4.4 ± 0.4	2.9–6.6
Sdr	0.9 ± 0.1	0.0–3.3	0.01 ± 0.0	0.00–0.01
Body composition				
% Fat thigh	44.4 ± 1.0	28.8–56.6	20.3 ± 1.7	12.5–27.1
% Lean thigh	53.6 ± 0.9	42.0–69.1	29.0 ± 1.9	19.9–37.0
% Fat subregion	36.8 ± 1.2	18.5–53.7	68.5 ± 1.8	61.2–77.1
3D ultrasound				
Dermal thickness	1.5 ± 0.0	1.2–2.1	1.7 ± 0.1	1.2–2.0
Ultrasound surface area	352 ± 8	259–470	335 ± 20	283–460
Surface texture photography:				
red-band SD	14.8 ± 0.5	6.8–22.7	14.9 ± 1.6	9.7–24.0
Biomechanical properties				
Laxity	1.1 ± 0.0	0.6–1.8	1.0 ± 0.1	0.7–1.3
Laxity %	62.0 ± 0.9	41.8–72.3	60.9 ± 2.2	50.3–69.6
Elastic deformation	1.8 ± 0.0	1.2–2.6	1.7 ± 0.1	1.4–2.0
Stiffness	143 ± 2	115–176	146 ± 4	125–158
Energy absorption	91.2 ± 1.4	67.3–121.4	87.9 ± 2.9	78.2–99.4
Elasticity (mm)	1.0 ± 0.0	0.6–1.5	1.0 ± 0.1	0.8–1.4
% Elasticity	55.3 ± 0.8	43.1–70.8	58.4 ± 2.0	51.7–68.2

of the dermal-subcutaneous border (ultrasound surface area, red-band SD from compressed images). Cellulite severity was associated positively with tissue compliance (energy absorption) and negatively with stiffness (less stiff, greater severity).

The parameters that predict cellulite severity were identified from multiple linear regression modeling procedures. Expert image score and *Svm* were selected as the quantitative measures of cellulite severity (dependent variable). The expert image score could be predicted from subregion % fat ($p < 0.001$) and *Sdr* ($p = 0.01$), giving the equation: *Image Score = −4.2 + (0.22 · Subregion % Fat) + (0.91 · Sdr)*. The values of R, R^2, and adjusted R^2 were 0.82, 0.68, and 0.67, respectively. Cellulite severity (*Svm*) could be predicted from subregion % fat ($p < 0.001$) and the dermal-subcutaneous surface area

Table V
Significant Correlations ≈ 0.4 or Higher (n = 56 subjects)

Parameter	Positively correlated with....
Expert image score	BMI, weight, thigh circumference, Svm, Sz, Spm, Sa, Sq, Sp, St, visual grade, thigh % fat, thigh subregion % fat, red-band SD, energy absorption
Svm	BMI, weight, thigh circumference, expert image score, visual grade, thigh % fat, thigh subregion % fat, ultrasound surface area, stiffness (neg),* energy absorption, red-band SD
Sz	BMI, weight, thigh circumference, expert image score, visual grade, thigh % fat, thigh subregion % fat
Visual grade	BMI, weight, thigh circumference, Sa, Sq, Spm, Svm, Sz, thigh % fat, thigh subregion % fat, ultrasound surface area, red-band SD, stiffness (neg), energy absorption
Age	% elasticity (neg)
Thigh subregion % fat	BMI, weight, thigh circumference, Sa, Sq, St, Spm, Svm, thigh % fat, ultrasound surface area, red-band SD, elastic deformation, energy absorption
Ultrasound surface area	BMI, weight, thigh circumference, Svm, Sz, thigh % fat, red-band SD, elastic deformation, energy absorption, stiffness (neg)
Elastic deformation	BMI, weight, thigh circumference, Spm, thigh % fat, ultrasound surface area, laxity %, laxity (mm), stiffness (neg), energy absorption, elasticity (mm)
Energy absorption	BMI, weight, thigh circumference, St, Spm, Svm, Sz, thigh % fat, ultrasound surface area, laxity (mm), elastic deformation, stiffness (neg), elasticity (mm)

* Neg: negative correlation.

(p = 0.02). The equation was: *Svm = −2.2 + (0.08 · Subregion % Fat) + (0.006 · D-S surface area)*, with R, R^2, and adjusted R^2 values of 0.68, 0.46, and 0.44, respectively.

MALE AND FEMALE COMPARISONS

Ten females, matched for BMI and age, were selected at random for comparison to the males. A second group of BMI- and age-matched females was used to further verify the results. The average BMI (kg/m^2) for the males was 33.2 ± 6, compared to 33.4 ± 6 and 33.0 ± 5.9 for the two female groups. *T*-test analyses confirmed that the groups were comparable for BMI and age.

The males and females differed significantly in body composition ($p < 0.001$) (Table IV). The mean subregion % fat was 20.3 ± 5.4% for the males and 36.5 ± 7.2% and 33.8 ± 9.3% for the females. The mean thigh % fat was 29.0 ± 6.1% for males and 44.5 ± 5.8% and 42.0 ± 7.3% for females. The mean live visual cellulite grade was directionally higher (p = 0.10) for one female group than for the males. No significant differences were found for the expert image score, thigh circumference, dermal thickness, dermal-subcutaneous surface areas, and biomechanical properties. With respect to cellulite severity, the males and females differed significantly in *Sdr* ($p < 0.005$), with substantially higher values for females (Figure 5).

DISCUSSION

Three-dimensional skin surface microstructures, e.g., wrinkles, have been quantified by various techniques (27–30). Many use surface replicas coupled with mechanical, laser,
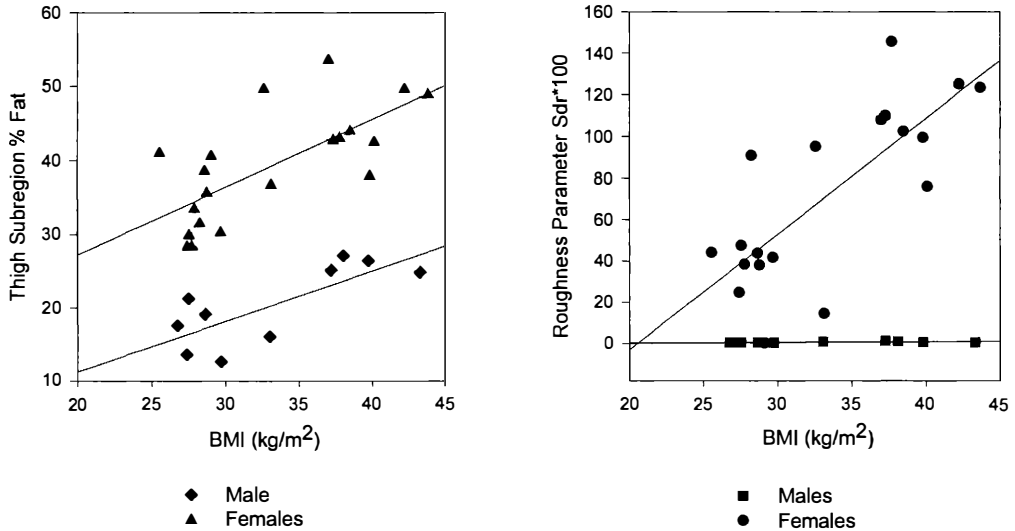
Figure 5. Male and female comparisons. Males had a significantly lower percent fat in the thigh subregion and significantly lower values for Sdr at comparable body mass indices. The graph shows $Sdr \cdot 100$ for clarity of illustration. For thigh subregion fat versus BMI, the correlation coefficients were 0.77 ($p = 0.01$) for males and 0.78 ($p < 0.001$) for females. For roughness Sdr versus BMI, the correlation coefficients were 0.69 ($p = 0.03$) for males and 0.77 ($p < 0.001$) for females.

optical or interference fringe profilometry to determine roughness parameters. For cellulite, the area of interest is large and the limitations of replica methods become significant. Akazaki et al. (28) described an optical system for direct skin surface measurements over a 6.4-mm^2 area with a high resolution of 12.5 µm. Optical profilometry with CCD sensors allows measurement of depths up to 6 mm (27), and interference fringe projection methods have a 1-mm depth of field (29). These distances are smaller than those encountered with cellulite. Three-dimensional skin surface features have been reported using the non-contact PRIMOS system, which projects parallel stripes onto the surface and determines the third dimension from differences in elevation between the projections and the skin (31,32). Quantitative roughness parameters in the µm range and within a sampling area of 2.4 × 3.0 cm can be measured by this method, indicating the suitability for microtextures.

The three-dimensional features of the face and head have been measured with non-contact laser surface-scanning systems that record the x, y, z coordinates of multiple points across the surface (33,34). Changes in the range of 2–3 mm could be accurately measured over a relatively large surface area. Rohmer et al. (35) recently used fringe projection methods to quantify the roughness parameters and volume of cellulite-affected skin. A system to directly measure 3D surface features and quantify wrinkle depth and width has been reported (28). Wrinkle depth was defined as the maximum distance from top to bottom, similar to St (vertical distance from the highest peak to the deepest valley) in this report. We used a non-contact three-dimensional laser surface scanner (resolution of 0.5 mm) to compute roughness and to provide a standardized, reproducible measure of severity. This system has been used to quantify the surface features of wounds and burn scars and to generate 3D data for the construction of burn masks (36). Since the laser-scanning technique does not use shadows to create the 3D

image, difficulties with lighting were avoided. The 3D images could easily be rotated with the software to provide the investigator with multiple views of the cellulite-affected skin. The subject's position on a rigid platform provided natural thigh compression.

The roughness parameters Svm and Sdr were highly correlated with the expert image scores for ten standard images and were, therefore, designated as the quantitative measures of cellulite severity. The strength of the agreements (a) between expert image scores and roughness values and (b) between live visual scores and the roughness parameters strongly indicates that the 3D laser scanning and analysis methodology quantitatively characterizes cellulite. The naïve judge and expert grades were highly correlated (r = 0.96) for the ten images, using the 0–9 scale. Svm and Sdr had the highest correlations to expert and naïve scores (r $\geq$ 0.86) (Figure 3). The strength of the correlations among naïve grades, expert grades, and roughness measures confirms that the data quantitatively assesses human perception of cellulite and can, therefore, be used to guide development and evaluation of treatment modalities. To our knowledge, this is the first report of a quantitative assessment of cellulite using 3D laser-scanning technology that also establishes the relationships between quantitative measurements of cellulite severity and human perception of the condition.

A combination of biophysical techniques, including standardized, expert clinical grading of photographs (wrinkling, rhytids, laxity/tone, etc), roughness parameters (Ra, Rz) from replicas, and subject assessment of improvement, has been used successfully to evaluate treatments on photodamaged facial skin (37). Rao *et al.* (15) used a combination of high-quality digital photography (multiple angles, tangential lighting), expert image scoring (four trained dermatologists), and subject self-assessment in a paired-comparison design to evaluate cellulite treatments. Surface features were captured from shadows at various angles, but quantitative roughness values were not reported. Bertin *et al.* (6) concluded that a combination of techniques, including surface macrotexture, biomechanical properties, cutaneous flowmetry, and dermal/hypodermal structure determination, were effective in measuring the effect of treatments on cellulite.

We found that cellulite severity, measured by expert image evaluation or quantitative surface roughness parameters, was significantly related to the body fat in the affected region, the architecture (surface area) of the dermal-subcutaneous border, and the tissue mechanical properties (compliance, stiffness). The body mass index and correlated anthropomorphic parameters (weight, thigh circumference) were highly associated with cellulite severity. The observed appearance of cellulite, i.e., cellulite severity as measured by surface roughness parameters, depended upon the percent fat in the thigh and the surface area of the dermal-subcutaneous junction. Cellulite severity was *predicted* by the percent fat in the subregion and the area of the dermal-subcutaneous border. While the biomechanical properties of energy absorption and stiffness correlated with surface roughness, they did not significantly add to the severity. The contributions of subcutaneous fat to cellulite were reported by Mole *et al.* (38). High-frequency ultrasound coupled with a patient questionnaire indicated that cellulite is caused by defects in adipocyte biology and the superficial fat tissues. Furthermore, the comparison of parameters for females and BMI- and age-matched males provided key information regarding the factors that influence cellulite. The outcomes suggest that percent thigh fat and surface area roughness deviation are the distinguishing features of cellulite, given the control for BMI and age in the comparisons. The identification of regional subcutaneous fat and the surface area of the dermal-subcutaneous border as the factors responsible for

the visual appearance of cellulite and the perception of severity will further guide the development of effective treatment modalities.

REFERENCES

(1) B. M. Kinney, Discussion—Cellulite treatment: A myth or reality: A prospective randomized, controlled trial of two therapies, endermologie and aminophylline cream, *Plast. Reconstr. Surg.,* 104, 1115–1117 (1999).

(2) Z. D. Draelos and K. D. Marenus, Cellulite: Etiology and purported treatment, *Dermatol. Surg.,* 23, 1177–1181 (1997).

(3) W. P. Smith, Cellulite treatments: Snake oils or skin science, *Cosmet. Toiletr.,* 110, 61–70 (1995).

(4) N. Collis, L. A. Elliot, C. Sharpe, and D. T. Sharpe, Cellulite treatment: A myth or reality: A prospective randomized, controlled trial of two therapies, endermologie and aminophylline cream, *Plast. Reconstr. Surg.,* 104, 1110–1114; discussion 1115–1117 (1999).

(5) R. M. DiSalvo, Controlling the appearance of cellulite, *Cosmet. Toiletr.,* 110, 50–59 (1995).

(6) C. Bertin, H. Zunino, J. C. Pittet, P. Beau, P. Pineau, M. Massonneau, C. Robert, and J. Hopkins. A double-blind evaluation of the activity of an anti-cellulite product containing retinol, caffeine, and ruscogenine by a combination of several non-invasive methods, *J. Cosmet. Sci.,* 52, 199–210 (2001).

(7) A. B. Rossi and A. L. Vergnanini, Cellulite: A review, *J. Eur. Acad. Dermatol. Venereol.,* 14, 251–262 (2000).

(8) G. W. Lucassen, W. L. N. van der Sluys, J. J. van Herk, A. M. Nuijs, P. E. Wierenga, A. ●. Barel, and R. Lambrecht, The effectiveness of massage treatment on cellulite as monitored by ultrasound imaging, *Skin Res. Technol.,* 3, 154–160 (1997).

(9) F. Perin, C. Perrier, J. C. Pittet, P. Beau, S. Schnebert, and P. Perrier, Assessment of skin improvement treatment efficacy using the photograding of mechanically-accentuated macrorelief of thigh skin, *Int. J. Cosmet. Sci.,* 22, 147–156 (2000).

(10) W. Hu, E. C. Siegfried, and D. M. Siegel, Product-related emphasis of skin disease information online, *Arch. Dermatol.,* 138, 775–780 (2002).

(11) J. S. Artz and M. I. Dinner, Treatment of cellulite deformities of the thighs with topical aminophylline gel, *Can. J. Plast. Surg.,* 3, 190–192 (1995).

(12) D. M. Hexsel and R. Mazzuco, Subcision: A treatment for cellulite, *Int. J. Dermatol.,* 39, 539–544 (2000).

(13) A. Kligman, A. Pagnoni, and T. Stoudemayer, Topical retinol improves cellulite, *J. Dermatol. Treat.,* 10, 119–125 (1999).

(14) C. Pierard-Franchimont, G. E. Pierard, F. Henry, V. Vroome, and G. Cauwenbergh, A randomized, placebo-controlled trial of topical retinol in the treatment of cellulite, *Am. J. Clin. Dermatol.,* 1, 369–374 (2000).

(15) J. Rao, K. E. Paabo, and M. P. Goldman, A double-blinded randomized trial testing the tolerability and efficacy of a novel topical agent with and without occlusion for the treatment of cellulite: A study and review of the literature, *J. Drugs Dermatol.,* 3, 417–425 (2004).

(16) M. Lis-Balchin, Parallel placebo-controlled clinical study of a mixture of herbs sold as a remedy for cellulite, *Phytotherapy Res.,* 13, 627–629 (1999).

(17) M. Rosenbaum, V. Prieto, J. Hellmer, M. Boschmann, J. Krueger, R. L. Leibel, and A. G. Ship, An

exploratory investigation of the morphology and biochemistry of cellulite, *Plast. Reconstr. Surg.,* **101,** 1934–1939 (1998).

(18) E. H. Rose, L. M. Vistnes, and G. Ksander, A microarchitectural model of regional variations in hypodermal mobility in porcine and human skin. *Ann. Plast. Surg.,* **2,** 252–266 (1978).

(19) F. Nurnberger and G. Muller, So-called cellulite: An invented disease, *J. Dermatol. Surg. Oncol.,* **4,** 221–229 (1978).

(20) G. E. Pierard, J. L. Nizet, and C. Pierard-Franchimont, Cellulite: From standing fat herniation to hypodermal stretch marks, *Am. J. Dermatopathol.,* **22,** 34–37 (2000).

(21) B. I. Dickinson and M. L. Gora-Harper, Aminophylline for cellulite removal, *Ann. Pharmacother.,* **30,** 292–293 (1996).

(22) http://www.predev.com, *Surface Metrology Guide* (2003).

(23) C. Walton, B. Lees, D. Crook, M. Worthington, I. F. Godsland, and J. C. Stevenson, Body fat distribution, rather than overall adiposity, influences serum lipids and lipoproteins in healthy men independently of age, *Am. J. Med.,* **99,** 459–464 (1995).

(24) J. Serup, J. Keiding, A. Fullerton, M. Gniadecka, and R. Gniadecki, "High-Frequency Ultrasound Examination of Skin: Introduction And Guide," in *Handbook of Non-Invasive Methods and the Skin,* J. Serup and B. E. Jemec, Eds. (CRC Press, Boca Raton, FL, 1995), pp. 239–256.

(25) M. K. Dobke, B. DiBernardo, C. Thompson, and U. Hakan, Assessment of biomechanical skin properties: Is cellulitic skin different? *Aesthet. Surg. J.,* **22,** 260–267 (2002).

(26) K. Denecker, P. De Neve, S. Van Assche, R. Van de Walle, I. Lemahieu, and W. Philips, Psychovisual evaluation of Lossy CMYK image compression for printing applications, *Computer Graphics Forum,* **21,** 5–17 (2002).

(27) J. L. Leveque, EEMCO guidance for the assessment of skin topography (European Expert Group on Efficacy Measurement of Cosmetics and Other Topical Products), *J. Eur. Acad. Dermatol. Venereol.,* **12,** 103–114 (1999).

(28) S. Akazaki, H. Nakagawa, H. Kazama, ●. Osanai, M. Kawai, Y. Takema, and G. Imokawa, Age-related changes in skin wrinkles assessed by a novel three-dimensional morphometric analysis, *Br. J. Dermatol.,* **147,** 689–695 (2002).

(29) J. M. Lagarde, C. Rouvrais, D. Black, S. Diridollou, and Y. Gall, Skin topography measurement by interference fringe projection: A technical validation, *Skin Res. Technol.,* **7,** 112–121 (2001).

(30) T. W. Fischer, W. Wigger-Alberti, and P. Elsner, Direct and non-direct measurement techniques for analysis of skin surface topography, *Skin Pharmacol. Appl. Skin Physiol.,* **12,** 1–11 (1999).

(31) U. Jacobi, M. Chen, G. Frankowski, R. Sinkgraven, M. Hund, B. Rzany, W. Sterry, and J. Lademann, *In vivo* determination of skin surface topography using an optical 3D device, *Skin Res. Technol.,* **10,** 207–214 (2004).

(32) P. M. Friedman, G. R. Skover, G. Payonk, A. N. Kauvar, and R. G. Geronemus, 3D in-vivo optical skin imaging for topographical quantitative assessment of non-ablative laser technology, *Dermatol. Surg.,* **28,** 199–204 (2002).

(33) J. P. Moss, S. F. Ismail, and R. J. Hennessy, Three-dimensional assessment of treatment outcomes on the face, *Orthod. Craniofac. Res.,* **6**(Suppl 1), 126–131; discussion 179–182 (2003).

(34) R. J. Hennessy, A. Lane, A. Kinsella, C. Larkin, E. O'Callaghan, and J. L. Waddington, 3D morpho-metrics of craniofacial dysmorphology reveals sex-specific asymmetries in schizophrenia, *Schizophr. Res.,* **67,** 261–268 (2004).

(35) E. Rohmer, S. Mac-Mary, D. Marsaut, J. Sainthillier, T. Ghabri, and P. Humbert, Fringes projection and cellulite, *Skin. Res. Technol.,* **10,** 1–16 (2004).

(36) J. Whitestone, G. Geisen, and B. McQuiston, Three-dimensional anthropometric techniques applied to the fabrication of burn masks and the quantification of wound healing, *SPIE* (San Diego, CA, 1996).

(37) S. S. Traikovich, Use of topical ascorbic acid and its effects on photodamaged skin topography, *Arch. Otolaryngol. Head Neck Surg.,* **125,** 1091–1098 (1999).

(38) B. Mole, P. Blanchemaison, D. Elia, M. Lafontan, J. Mauriac, M. Mauriac, S. Mimoun, and J. Raison, High frequency ultrasonography and celluscore: An improvement in the objective evaluation of cellulite phenomenon, *Ann. Chir. Plast. Esthet.,* **49,** 387–395 (2004).